Detecting an Upward Terrestrial Gamma-Ray Flash from its Reverse Positron Beam

John Ortberg[1], David M. Smith[1], Joseph Li[2], Joseph Dwyer[3], Gregory Bowers[4]

[1]Physics Department and Santa Cruz Institute for Particle Physics, University of California, Santa Cruz, California, USA
[2]Saratoga High School, Saratoga, California, USA
[3]Department of Physics and Space Science Center (EOS), University of New Hampshire, Durham, New Hampshire, USA
[4]Los Alamos National Laboratory, Los Alamos, NM, USA

Key Points:

- An upward directed terrestrial gamma-ray flash produces a reverse beam with 1% of the brightness of the main beam.
- GEANT4 simulations show that the downward beam could be easily detectable at an altitude 1 km or greater.
- Coastal mountainous regions in the tropics would be good candidates for this reverse beam detection.

Corresponding author: John Ortberg, jortberg@westmont.edu

Abstract

In 2015, Bowers et al. (2018, https://doi.org/10.1029/2017JD027771) detected a terrestrial gamma-ray flash (TGF) in Hurricane Patricia from an aircraft flying at 2.6 km through what they argued to be a beam of downward gamma radiation produced by the positron component of the TGF. This paper uses the energy spectrum for gamma rays produced by the positrons of a relativistic runaway electron avalanche as simulated by the REAM code, propagated through a model of the Earth's atmosphere in Geant4, to examine the feasibility of detecting a typical upward TGF through its reverse positron beam at various altitudes on the ground. We find that, with patience, modest-sized scintillators on mountains as low as 1 km should be able to observe the same TGFs seen from spacecraft.

1 Background & Summary

Terrestrial gamma-ray flashes (TGFs) are extremely short, intense bursts of gamma rays caused by an avalanche of electrons accelerated to relativistic speeds inside thunderclouds (and coincident with lightning). TGFs were first detected via satellite on the Compton Gamma-Ray Observatory's Burst And Transient Source Experiment (Fishman et al., 1994), where they stood out as being being brighter than all other gamma-ray activity on Earth combined (Fishman et al., 2011; Dwyer et al., 2010). In addition to the insight TGFs provide into the activity and fields inside thunderstorms, they are of interest to the community because of their potential to deliver dangerous doses of radiation. Dwyer et al. (2010) calculated that a pilot flying above the avalanche region of a TGF could receive a dose equivalent to up to 400 chest X-rays (0.03 Sv).

1.1 Positron Production inside the Avalanche Region

Inside the source region of a TGF, the electric field is strong enough to overpower the drag force on high energy electrons and accelerate them until they approach the speed of light (Wilson, 1925). These electrons quickly gain enough energy to occasionally knock other (bound) electrons free at relativistic energies in a chain reaction (Gurevich et al., 1992) that can result in the initial electrons multiplying in number on the order of up to 10^5 (known as the *avalanche multiplication factor*) (Dwyer, 2008; Dwyer, 2012). That phenomenon, which is not exclusive to TGFs, is known as a relativistic runaway electron avalanche (RREA). The gamma rays produced by the bremsstrahlung of these electrons (mostly toward the end of the avalanche region) reach very high energies ($\gg$ 1 MeV) and will therefore produce positron/electron pairs on occasion. This pair production is significant; if it occurs within the high-field region, the new positron will be accelerated to relativistic speeds in the opposite direction.

Since there are no bound positrons to be knocked out of an atom, positrons do not multiply by avalanching the way electrons do. Each time an electron undergoes Møller scattering it not only loses energy itself, but also introduces a new electron, energetic enough to run away but much less energetic than the evolved runaway population. Therefore the positrons and their associated bremsstrahlung gammas have a higher average energy after being accelerated the entire length of the avalanche region, even though there are far fewer of them relative to the electrons. This results in not only higher-energy bremsstrahlung photons, but a more efficient conversion of the particle energy to bremsstrahlung radiation relative to ionization losses. The net result is that the reverse beam has about 1% of the number of gamma-rays in the main, forward beam. The spectra of the two beams are compared in Figure 1.

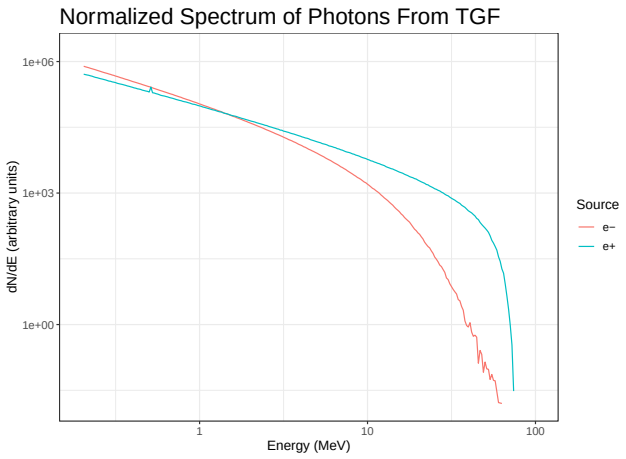

Figure 1. The spectrum of gammas created by positrons from a TGF is slightly harder than the spectrum created by electrons in the 100 keV to 100 MeV range plotted here. Each spectrum is normalized to have the same total number of photons - note that in a TGF there about 100 times as many photons created by electrons as positrons.

1.2 TGF Detection

On the order of 1,000 upward-directed TGFs occur per day that could be visible by satellite (Briggs et al., 2013), and possibly more if an undetected population of slightly fainter ones exists (Albrechtsen et al., 2019). An estimate for the frequency of downward-directed TGFs does not exist. Only a handful have ever been detected on the ground if that definition is restricted to events believed to be fully as bright as TGFs seen from orbit, and these events have mostly been associated with upward leaders from rocket wires or towers (Dwyer et al., 2004; Hare et al., 2016; Bowers et al., 2017; Enoto et al., 2017; Wada et al., 2019). But thousands of upward directed TGFs, which generally occur at altitudes of around 10–15 km (Dwyer & Smith, 2005; Stanley et al., 2006; Shao et al., 2010; Lu et al., 2010; Cummer et al., 2014, 2015), have been detected by satellites (Fishman et al., 1994; Grefenstette et al., 2009; Briggs et al., 2013; Gjesteland et al., 2014; Marisaldi et al., 2014; Østgaard et al., 2019). They produce on the order of $10^{16} - 10^{17}$ upward bremsstrahlung gammas above 1 MeV from electrons (Dwyer & Smith, 2005). And while there are generally 1000 times as many electrons as positrons in a TGF source, positrons produce about 10 times as many gammas in this process as a result of having higher average energy and traveling larger distances on average than the runaway electrons, according to the Relativistic Electron Avalanche Mode (REAM) simulation code of Dwyer (2003). Additionally, the gammas produced by the positrons having a slightly harder spectrum (as seen in Figure 1) results in less Compton scattering in the atmosphere. For this reason, the detectability of the reverse beam at a given amount of intervening atmosphere should be better than the 1:100 gamma-ray ratio relative to the upward beam implies. In this paper, we investigate if the decreased brightness of the downward beam could be offset not only by this effect but by the fact that a detector on the ground would be much closer to the source.

1.3 Reverse Beam Detection Suspected in Hurricane Patricia

The idea that a TGF could have a reverse beam due to positron bremsstrahlung has been known to be possible in theory given the simulations presented in Dwyer (2008), though the feasibility of detecting such a reverse beam has not been explored in detail. Recently Bowers et al. (2018) believe they observed this phenomenon in the eyewall of

Hurricane Patricia in the 2015 season. A TGF was detected onboard an aircraft at 2.6 km altitude, but the radio signal for the associated lightning strike suggested an upward motion of electrons (and therefore upward directed TGF). The intensity of the reverse bremsstrahlung beam observed was consistent with a model of a TGF that would have had an ordinary luminosity if observed from above from space. The observed spectrum was consistent with both a direct and reverse TGF bremsstrahlung beam due to limited photon counting statistics.

2 Methods

REAM is a Monte Carlo simulation of the avalanche region of an electric field in the air (Dwyer, 2003; Dwyer & Smith, 2005). Seed electrons of the RREA spectrum $\exp(-\frac{E}{7.3MeV})$ are injected into a high field region of 7 avalanche lengths. For a 12 km TGF with $\vec{E} = -400\frac{kV}{m}\hat{z}$, this is a length of approximately 400 meters.

We chose a "standard" TGF for our calculations as one producing $1{\times}10^{17}$ gamma-rays of energy >1 MeV in the primary (upward) beam. This corresponds to 3×10^{17} relativistic electrons in the avalanches according to the REAM code (Dwyer et al., 2017) assuming an electric field in the avalanche region of 400 kV/m sea level equivalent. Mailyan et al. (2016) analyzed 40 individual TGFs observed by the *Fermi* spacecraft and found, using the same REAM model, numbers of relativistic electrons ranging from 4×10^{16} to 3×10^{19} electrons, with a median value of around 8×10^{17} (Figure 8a of their paper). As this range of values is sensitive to the best-fit production altitudes, we consider our value of $3{\times}10^{17}$ electrons to be suitably conservative for this study. When Mailyan et al. (2016) used a uniform production altitude of 13.6 km, $3{\times}10^{17}$ electrons was close to the minimum number they found in the sample of 40 TGFs (their Figure 8b).

Positrons are created by bremsstrahlung gammas which are created by the relativistic electrons in the simulation. The output of the simulation for an RREA field region from 10.4 km to 12 km altitude is shown in Figure 2. Though the simulation keeps track of all positrons created, only those within the high field region will contribute to the downward beam — so that any positrons created above 12 km ($\sim 87.2\%$ of the total) can be ignored. The field in the simulation is infinite in the radial direction, so we keep track of the radial distance at which each positron is created. There is no consensus as to the radial extent of the high field region in a TGF, and any positron outside of the high field region will not contribute to the downward beam. However, since >95% of all potential runaway positrons are created within a 500 m radius of the avalanche center, any model in which the large-scale thundercloud field reaches the runaway threshold will yield virtually all of the modeled reverse beam.

We save the state of the bremsstrahlung gammas created by the runaway positrons mentioned above. This output includes photon energy, mass thickness ($\frac{g}{cm^2}$) of air traveled from the end of the avalanche region, position in the x-y plane, and the z-component of direction. For the z-component of position, we calculate each photon's altitude from mass thickness of air traveled as if the end of the avalanche region occurred at 8, 10, 12, and 14 km using appropriate air density from the *U.S. standard atmosphere* (1976). An azimuthal angle ϕ was randomly generated for each photon in our simulation to allow visualization of the detections in the x-y plane (as in Figure 3).

The photons from the REAM output are used as input (with associated position, direction, and energy) in CERN's Geant4 (GEometry ANd Tracking) software for particle physics (Agostinelli et al., 2003; Allison et al., 2016, 2006). An approximate model of Earth's atmosphere is derived by using 500 m tall slabs of constant density from the *U.S. standard atmosphere* (1976) extending from ground level to 20 km. Detection surfaces are placed at 0, 1, 2, 3, and 4 km altitude. While going higher would continue to increase the chance of observing an event, 4 km is a reasonable limit to how high one

can expect to find a location able to host a detector (our group recently delivered a detector to the High-Altitude Water Cherenkov Observatory (HAWC) at 4.1 km in southern Mexico (Shao et al., 2018).) EM Opt4, the Geant4 physics list that has the highest priority of accuracy over performance speed, was chosen to ensure accurate modeling in the 100 keV to 100 MeV range (Geant4 Collaboration, 2018).

It is worth noting that there are three primary models for the TGF mechanism. In one, the positrons and X-rays that travel 'upstream' knock enough new electrons free to sustain the avalanche in a feedback process (Dwyer, 2008; Dwyer, 2012). The $\vec{E}$-field in this model is relatively uniform in a large volume of space. In the second model, electric field enhancements near lightning leader/streamer tips provide moderately energetic seed electrons that subsequently undergo RREA in the large scale field (Moss et al., 2006; Dwyer, 2008). In both of these models, many positrons are produced by gamma-ray pair production within the region of high field where they can run away, which is the situation we model with REAM. But there are also models in which the seed electrons from the leader tip accelerate and avalanche entirely in a small region of high field around the tip (Moss et al., 2006; Carlson et al., 2009; Celestin & Pasko, 2011). In these models, pair production by gamma rays could occur largely outside the small volume in which the positrons could run away, suppressing the reverse bremsstrahlung beam.

3 Results

To get a reasonable minimum fluence that would be of interest, we consider a 3 in (7.62cm) diameter by 3 in long NaI detector (3"x 3") looking at energies > 50 keV. We modeled such a detector under the average spectrum of the reverse beam at 2 km altitude. The simulation was run under Geant3 (GEANT Team, 1993) using the full mass model for a balloon payload from the BARREL project (Millan et al., 2013), which includes a NaI detector of this shape, an aluminum frame, some electronics and a styrofoam box – a reasonable stand-in for a generic detector package that might be deployed to a mountain site. The mass model also included a ground surface made of SiO_2 underneath the detector package.

This scenario gives a detector effective area of about 49 cm^2, 15% of which comes from the detection of photons Compton scattered upwards by the ground. Our 5"x 5" NaI detector at HAWC (4.1 km elevation) receives a background count rate of about 0.2 photons/ms, which translates to 0.072 photons/ms when scaled by area to 3"x 3". Assuming the background follows a Poisson distribution, receiving 6 counts in a millisecond would be expected by chance about once in 63 days. Lightning data could then determine the authenticity of a low count event. Thus we chose 6 counts as a minimum, leading to a fluence threshold of 0.12 photons/cm^2 indicated by a horizontal red line in Figure 3. In the event that lightning data were not available and false positives could not be tolerated, a threshold of 8 counts (fluence threshold 0.16 photons/cm^2) would give a chance detection once in 2000 years.

The fluence will decrease for a given altitude the farther a detector is horizontally from the point directly under the TGF. Thus we define a "radius of detectability" inside which the fluence will always be above the 6 count threshold for a 3x3" NaI detector. This is best illustrated in the left panel of Figure 3.

For a detector at 4 km, the fluence rises up to a maximum of several hundred photons/cm^2. As a TGF normally takes place on the order of 10^{-4} seconds (Roberts et al., 2018), the flux at 4 km could be enough to paralyze a detector or at least cause significant dead time.

Table 1: Detectability of a downward 10 km TGF versus observation altitude

Alt. (km)	Radius of Detectability (km)	Area of Detectability (km^2)
1	0.7	1.4
2	1.8	10.2
3	2.4	17.4
4	2.7	23.0

The prominent central peak that appears in the 4 km detector in Figure 3 becomes more diffuse at lower altitudes. The horizontal spreading of the photons due to their angular distribution and the increased likelihood of Compton scattering through additional atmosphere (which gets increasingly dense) both contribute to this effect. Thus the radius of detectability is not solely a function of the intensity of the beam at any given altitude, and has a maximum around 2.5-3 km as seen in Figure 4.

The altitude at which a TGF occurs will have a significant impact on its flux at the surface. Cummer et al. (2014) and Cummer et al. (2015) report 5 TGFs associated with lightning leader tips around 8-12 km (however they do not conclude altitudes for the TGFs themselves). Simulations with TGF source heights at 8, 10, 12, and 14 km (see Figure 4) reveal that TGFs occuring at 14 km and above would not be detectable at altitudes of 1 km and below. The relative prevalence of different source altitudes as a function of location is unknown, however a general correlation with tropopause height is to be expected (Smith et al., 2010).

4 Discussion

Roberts et al. (2018) identified over 1000 TGFs recorded by the Fermi Space Telescope Gamma Ray Burst Monitor that were also located to specific lightning activity by the World-Wide Lightning Location Network (WWLLN). In addition to making the location data publicly available (Fermi Science Support Center; http://fermi.gsfc.nasa.gov/ssc/data/access/gbm/tgf), they examined the "coastline-distance distribution" and found that locations 0-80 km inland in tropical regions in general have the highest density of TGFs. A similar result was found by Albrechtsen et al. (2019). In general it seems that low-latitude, mountainous (≥ 1 km) regions within 80 km of a coast would make good candidate detector sites.

Searching the Fermi database, as many as 7-8 TGFs per square degree (see Figure 5) were found in some tropical regions over the 6 years of data collection. A rough estimation can be made of ρ_{tgf} (TGF per km^2 per year) for such regions. The parameters are broken down as shown in Table 2 and used as in equation 1. TGFs without a WWLLN match were not included in this analysis, as the TGF viewing radius of Fermi GBM (800 km) is much larger than 1 degree at the equator (111 km). It is also important to appreciate that some factors that influence thunderstorm development, such as distance to coastline and local topography, change on the 100 km distance scale.

$$\rho_{\mathrm{tgf}} = \frac{\rho_{\mathrm{Fermi}}}{f_{\mathrm{livetime}} \cdot \eta_{\mathrm{localization}}} = \frac{1.25 \times 10^{-4}}{1.7 \times 10^{-3} \cdot 0.32} \approx 0.2 \frac{\mathrm{TGF}}{\mathrm{km}^2 \cdot \mathrm{yr}} \tag{1}$$

Table 2: Parameters for calculating local TGF occurrence rates

Variable	Description	Value
ρ_{Fermi}	Density of TGFs per year per km^2 detected by Fermi	$1.25 \times 10^{-4} \frac{\text{TGF}}{\text{km}^2 \cdot \text{yr}}$
f_{livetime}	Fraction of time that a point can be detected by Fermi. This is calculated based on the latitude of these high density regions, given the 25.6° inclination and effective detectability radius of 425 km (Briggs et al., 2013; Smith et al., 2016). The latitudes of the high density regions were between 5° and 12°, leading to less than a 5% variation in f_{livetime}.	1.7×10^{-3}
$\eta_{\text{localization}}$	TGF localization efficiency: a WWLLN match was found for just under 1 in 3 TGFs, so on average there were just over 3 times as many TGFs in each degree than WWLLN matches.	0.32

Several detector altitude and TGF source height configurations produce an area of detectability in the tens of km^2, which would suggest an expected detection rate of several reverse beams per year.

5 Conclusion

Simulations suggest that a detector at an altitude of a few km would see significant counts from the downward positron beam of an upward directed TGF occurring within a few radial km of directly overhead at normal altitudes, with a > 2 km detector altitude being suitable for tropical TGFs happening at altitudes up to 14 km. Choosing such a high elevation site with high TGF frequency would be imperative to maximize the odds of making a detection. Further research into TGF source height and frequency by region is planned.

Acknowledgments

The authors wish to thank the World Wide Lightning Location Network (http://wwlln.net), a collaboration among over 50 universities and institutions, for providing the lightning location data used in this paper. JCO, JRD, and DMS acknowledge the support of National Science Foundation awards AGS-1612466, AGS-1160226, and AGS-1613028. The code and data files used in this work are available at http://research-archive.scipp.ucsc.edu/reversebeam/.

References

Agostinelli, S., Allison, J., Amako, K., Apostolakis, J., Araujo, H., Arce, P., ... G

EANT4 Collaboration (2003, July). G EANT4—a simulation toolkit. *Nuclear Instruments and Methods in Physics Research A*, *506*, 250-303. doi: 10.1016/S0168-9002(03)01368-8

Albrechtsen, K. H., Østgaard, N., Berge, N., & Gjesteland, T. (2019, January). Observationally Weak TGFs in the RHESSI Data. *Journal of Geophysical Research (Atmospheres)*, *124*, 287-298. doi: 10.1029/2018JD029272

Allison, J., Amako, K., Apostolakis, J., Araujo, H., Arce, P., Asai, M., ... Yoshida, H. (2006, 02). Geant4 developments and applications. *IEEE Transactions on Nuclear Science*, *53*, 270-278. doi: 10.1109/TNS.2006.869826

Allison, J., Amako, K., Apostolakis, J., Arce, P., Asai, M., Aso, T., ... Yoshida, H. (2016). Recent developments in geant4. *Nuclear Instruments and Methods in Physics Research Section A: Accelerators, Spectrometers, Detectors and Associated Equipment*, *835*, 186 - 225. Retrieved from `http://www.sciencedirect.com/science/article/pii/S0168900216306957` doi: https://doi.org/10.1016/j.nima.2016.06.125

Bowers, G. S., Smith, D. M., Kelley, N. A., MartinezâĂŘMcKinney, G. F., Cummer, S. A., Dwyer, J. R., ... Rassoul, H. K. (2018). A Terrestrial Gamma-Ray Flash inside the Eyewall of Hurricane Patricia. *J. Geophys. Res.*, *123*. doi: https://doi.org/10.1029/2017JD027771

Bowers, G. S., Smith, D. M., Martinez-McKinney, G. F., Kamogawa, M., Cummer, S. A., Dwyer, J. R., ... Kawasaki, Z. (2017, October). Gamma Ray Signatures of Neutrons From a Terrestrial Gamma Ray Flash. *Geophys. Res. Let.*, *44*, 10. doi: 10.1002/2017GL075071

Briggs, M. S., Xiong, S., Connaughton, V., Tierney, D., Fitzpatrick, G., Foley, S., ... Hutchins, M. L. (2013, June). Terrestrial gamma-ray flashes in the Fermi era: Improved observations and analysis methods. *Journal of Geophysical Research (Space Physics)*, *118*, 3805-3830. doi: 10.1002/jgra.50205

Briggs, M. S., Xiong, S., Connaughton, V., Tierney, D., Fitzpatrick, G., Foley, S., ... Hutchins, M. L. (2013, 6). Terrestrial gammaâĂŘray flashes in the fermi era: ImprovedâĂĽobservations and analysis methods. *Journal of Geophysical Research: Space Physics*, *118*(6), 3805–3830. Retrieved from `https://doi.org/10.1002/jgra.50205` doi: 10.1002/jgra.50205

Carlson, B. E., Lehtinen, N. G., & Inan, U. S. (2009, December). Terrestrial gamma ray flash production by lightning current pulses. *Journal of Geophysical Research (Space Physics)*, *114*, 0. doi: 10.1029/2009JA014531

Celestin, S., & Pasko, V. P. (2011, March). Energy and fluxes of thermal runaway electrons produced by exponential growth of streamers during the stepping of lightning leaders and in transient luminous events. *Journal of Geophysical Research (Space Physics)*, *116*, 3315. doi: 10.1029/2010JA016260

Cummer, S. A., Briggs, M. S., Dwyer, J. R., Xiong, S., Connaughton, V., Fishman, G. J., ... Solanki, R. (2014, December). The source altitude, electric current, and intrinsic brightness of terrestrial gamma ray flashes. *Geophys. Res. Let.*, *41*, 8586-8593. doi: 10.1002/2014GL062196

Cummer, S. A., Lyu, F., Briggs, M. S., Fitzpatrick, G., Roberts, O. J., & Dwyer, J. R. (2015, Sep). Lightning leader altitude progression in terrestrial gamma-ray flashes. *Geophysical Research Letters*, *42*, 7792-7798. doi: 10.1002/2015GL065228

Dwyer, J. R. (2003). A fundamental limit on electric fields in air. *Geophys. Res. Let.*, *30*(20), 2055.

Dwyer, J. R. (2008). Source mechanisms of terrestrial gamma-ray flashes. *J. Geophys. Res.*, *113*, D10103. doi: 10.1029/2007JD009248

Dwyer, J. R. (2012, February). The relativistic feedback discharge model of terrestrial gamma ray flashes. *Journal of Geophysical Research (Space Physics)*, *117*, 2308. doi: 10.1029/2011JA017160

Dwyer, J. R., Liu, N., Eric Grove, J., Rassoul, H., & Smith, D. M. (2017, Au-

gust). Characterizing the source properties of terrestrial gamma ray flashes. *Journal of Geophysical Research (Space Physics)*, *122*, 8915-8932. doi: 10.1002/2017JA024141

Dwyer, J. R., Rassoul, H., Al-Dayeh, M., Caraway, L., Chrest, A., Wright, B., ... Smyth, C. (2004). A ground level gamma-ray burst observed in association with rocket-triggered lightning. *Geophys. Res. Let.*, *31*, L05119. doi: 10.1029/2003GL018771

Dwyer, J. R., & Smith, D. M. (2005). A comparison between Monte Carlo simulations of runaway breakdown and terrestrial gamma-ray flash observations. *Geophys. Res. Let.*, *32*, L08811. doi: 10.1028/2005GL023848

Dwyer, J. R., Smith, D. M., Uman, M. A., Saleh, Z., Grefenstette, B., Hazelton, B., & Rassoul, H. K. (2010). Estimation of the fluence of high-energy electron bursts produced by thunderclouds and the resulting radiation doses received in aircraft. *J. Geophys. Res.*, *115*, D09206. doi: 10.1029/2009JD012039

Enoto, T., Wada, Y., Furuta, Y., Nakazawa, K., Yuasa, T., Okuda, K., ... Tsuchiya, H. (2017, November). Photonuclear reactions triggered by lightning discharge. *Nature*, *551*, 481-484. doi: 10.1038/nature24630

Fishman, G. J., Bhat, P. N., Mallozzi, R., Horack, J. M., Koshut, T., Kouveliotou, C., ... Christian, H. J. (1994). Discovery of intense gamma-ray flashes of atmospheric origin. *Science*, *264*, 1313-1316.

Fishman, G. J., Briggs, M. S., Connaughton, V., Bhat, P. N., Paciesas, W. S., von Kienlin, A., ... Greiner, J. (2011, July). Temporal properties of the terrestrial gamma-ray flashes from the Gamma-Ray Burst Monitor on the Fermi Observatory. *Journal of Geophysical Research (Space Physics)*, *116*, A07304. doi: 10.1029/2010JA016084

GEANT Team. (1993). *GEANT - Detector description and simulation tool, CERN program library long write-up W5013* (Tech. Rep.). CERN, Geneva.

Geant4 Collaboration. (2018). Physics list guide. (Available at `https://geant4.web.cern.ch/node/1731#opt4`)

Gjesteland, T., Østgaard, N., Nisi, R., Collier, A., Lu, G., Cummer, S., & Smith, D. (2014, May). Twelve Years of RHESSI TGFs - The second RHESSI TGF catalog. In *Egu general assembly conference abstracts* (Vol. 16, p. 14125).

Grefenstette, B., Smith, D., Hazelton, B., & Lopez, L. (2009). First RHESSI terrestrial gamma-ray flash catalog. *J. Geophys. Res.*, *114*, A02314. doi: 10.1029/2008JA013721

Gurevich, A. V., Milikh, G. M., & Roussel-Dupré, R. A. (1992). Runaway electron mechanism of air breakdown and preconditioning during a thunderstorm. *Physics Letters A*, *165*, 463.

Hare, B. M., Uman, M. A., Dwyer, J. R., Jordan, D. M., Biggerstaff, M. I., Caicedo, J. A., ... Bozarth, A. (2016, June). Ground-level observation of a terrestrial gamma ray flash initiated by a triggered lightning. *Journal of Geophysical Research (Atmospheres)*, *121*, 6511-6533. doi: 10.1002/2015JD024426

Lu, G., Blakeslee, R. J., Li, J., Smith, D. M., Shao, X.-M., McCaul, E. W., ... Cummer, S. A. (2010). Lightning mapping observation of a terrestrial gamma-ray flash. *Geophys. Res. Let.*, *37*, L11806. doi: 10.1029/2010GL043494

Mailyan, B. G., Briggs, M. S., Cramer, E. S., Fitzpatrick, G., Roberts, O. J., Stanbro, M., ... Dwyer, J. R. (2016, November). The spectroscopy of individual terrestrial gamma-ray flashes: Constraining the source properties. *Journal of Geophysical Research (Space Physics)*, *121*, 11. doi: 10.1002/2016JA022702

Marisaldi, M., Fuschino, F., Tavani, M., Dietrich, S., Price, C., Galli, M., ... Vercellone, S. (2014, February). Properties of terrestrial gamma ray flashes detected by AGILE MCAL below 30 MeV. *Journal of Geophysical Research (Space Physics)*, *119*, 1337-1355. doi: 10.1002/2013JA019301

Millan, R. M., McCarthy, M. P., Sample, J. G., Smith, D. M., Thompson, L. D., McGaw, D. G., ... Hudson, M. K. (2013, Nov). The Balloon Array for

RBSP Relativistic Electron Losses (BARREL). , *179*(1-4), 503-530. doi: 10.1007/s11214-013-9971-z

Moss, G. D., Pasko, V. P., Liu, N., & Veronis, G. (2006). Monte carlo model for analysis of thermal runaway electrons in streamer tips in transient luminous events and streamer zones of lightning leaders. *J. Geophys. Res.*, *111*, A02307.

Østgaard, N., Neubert, T., Reglero, V., Ullaland, K., Yang, S., Genov, G., ... Al-nussirat, S. (2019). First 10 months of tgf observations by asim. *Journal of Geophysical Research: Atmospheres*. Retrieved from `https://agupubs.onlinelibrary.wiley.com/doi/abs/10.1029/2019JD031214` doi: 10.1029/2019JD031214

Roberts, O. J., Fitzpatrick, G., Stanbro, M., McBreen, S., Briggs, M. S., Holzworth, R. H., ... Mailyan, B. G. (2018, May). The First Fermi-GBM Terrestrial Gamma Ray Flash Catalog. *Journal of Geophysical Research (Space Physics)*, *123*, 4381-4401. doi: 10.1029/2017JA024837

Shao, X.-M., Hamlin, T. D., & Smith, D. M. (2010). A closer examination of terrestrial gamma-ray flash-related lightning processes. *J. Geophys. Res.*, *115*, A00E30. doi: 10.1029/2009JA014835

Shao, X.-M., Ho, C., Caffrey, M., Graham, P., Haynes, B., Bowers, G., ... Rassoul, H. (2018). Broadband rf interferometric mapping and polarization (bimap) observations of lightning discharges: Revealing new physics insights into breakdown processes. *Journal of Geophysical Research: Atmospheres*, *123*(18), 10,326-10,340. Retrieved from `https://agupubs.onlinelibrary.wiley.com/doi/abs/10.1029/2018JD029096` doi: 10.1029/2018JD029096

Smith, D. M., Buzbee, P., Kelley, N. A., Infanger, A., Holzworth, R. H., & Dwyer, J. R. (2016, October). The rarity of terrestrial gamma-ray flashes: 2. RHESSI stacking analysis. *Journal of Geophysical Research (Atmospheres)*, *121*, 11. doi: 10.1002/2016JD025395

Smith, D. M., Hazelton, B. J., Grefenstette, B. W., Dwyer, J. R., Holzworth, R. H., & Lay, E. H. (2010). Terrestrial gamma ray flashes correlated to storm phase and tropopause height. *Journal of Geophysical Research: Space Physics*, *115*(A8). Retrieved from `https://agupubs.onlinelibrary.wiley.com/doi/abs/10.1029/2009JA014853` doi: 10.1029/2009JA014853

Stanley, M. A., Shao, X., Smith, D. M., Lopez, L., Pongratz, M., Harlin, J., ... Regan, A. (2006). A link between terrestrial gamma-ray flashes and intracloud lightning discharges. *Geophys. Res. Let.*, *33*, L06803. doi: 10.1029/20005GL025537

U.S. standard atmosphere (Tech. Rep.). (1976, October).

Wada, Y., Enoto, T., Nakazawa, K., Furuta, Y., Yuasa, T., Nakamura, Y., ... Tsuchiya, H. (2019, Aug). Downward Terrestrial Gamma-Ray Flash Observed in a Winter Thunderstorm. , *123*(6), 061103. doi: 10.1103/PhysRevLett.123.061103

Wilson, C. T. R. (1925). The electric field of a thundercloud and some of its effects. *Phys. Soc. London Proc.*, *32D*, 37.

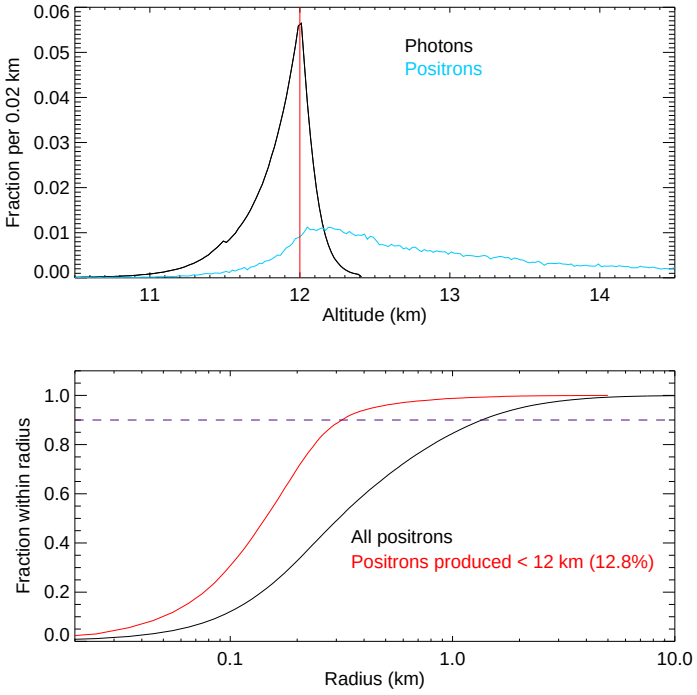

Figure 2. (top) Fraction of positrons and photons produced from an avalanche region extending from 10.4 km to 12 km altitude in REAM. Positrons produced above 12 km will not accelerate in the avalanche region. (bottom) Fraction of positrons created as a function of radial distance from the center of the avalanche. The red line is relevant to the reverse beam as only positrons produced below 12 km have the potential to accelerate downward in the avalanche region. The dashed line indicates 90% of the positron population. In both plots, 'fraction' refers to fraction of total photons/positrons in the simulated TGF.

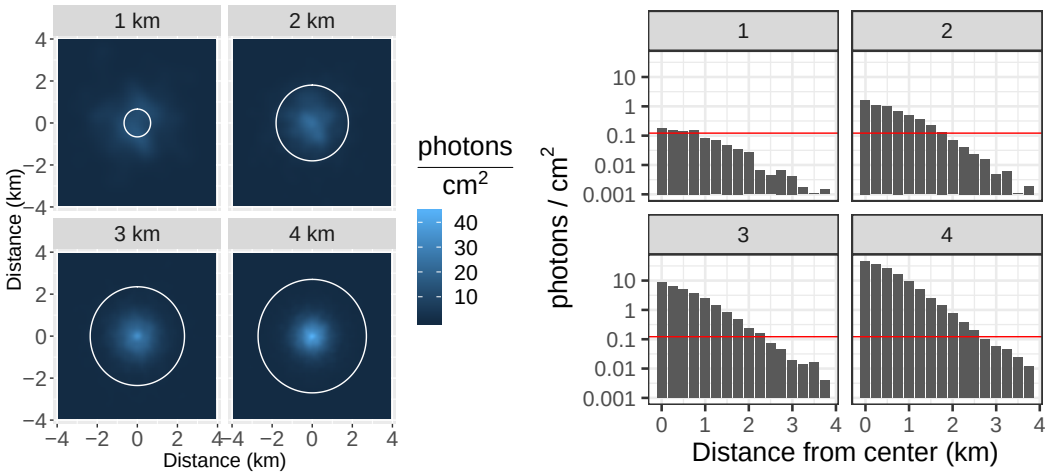

Figure 3. Simulation of a 10 km TGF. (left) Photon density (linear color scale) in the x-y plane at 4 altitudes; the white circles indicate the "radius of detectability". Kernal density estimation (KDE) is used for smoothing. (right) Histogram of fluence/area (logarithmic) vs. distance horizontally from the point beneath a TGF at 10 km – the red line indicates the detectability threshold of 0.12 photons/cm^2.

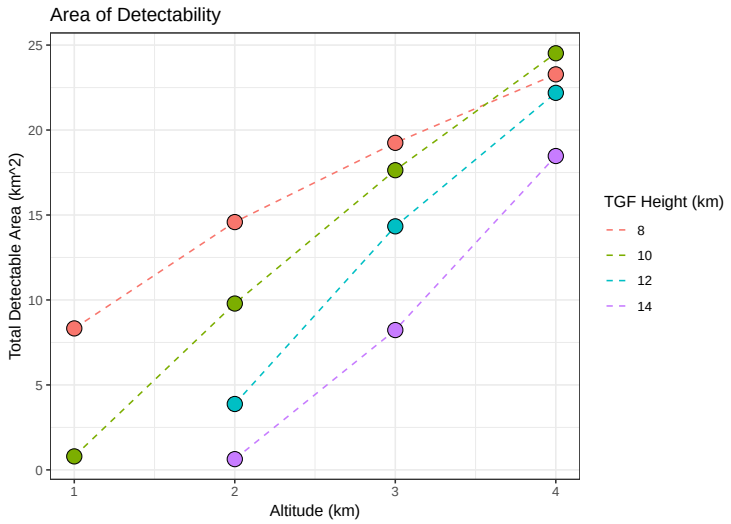

Figure 4. Four lines corresponding to four different TGF source altitudes illustrate the maximum area covered by a detector when placed at different elevations. The points are simulation results and the dotted lines are a simple linear interpolation. For detectable area 10 km^2 in a region that averages $0.1 \frac{TGF}{km^2 \cdot year}$, the expectation value would be 1 detection per year.

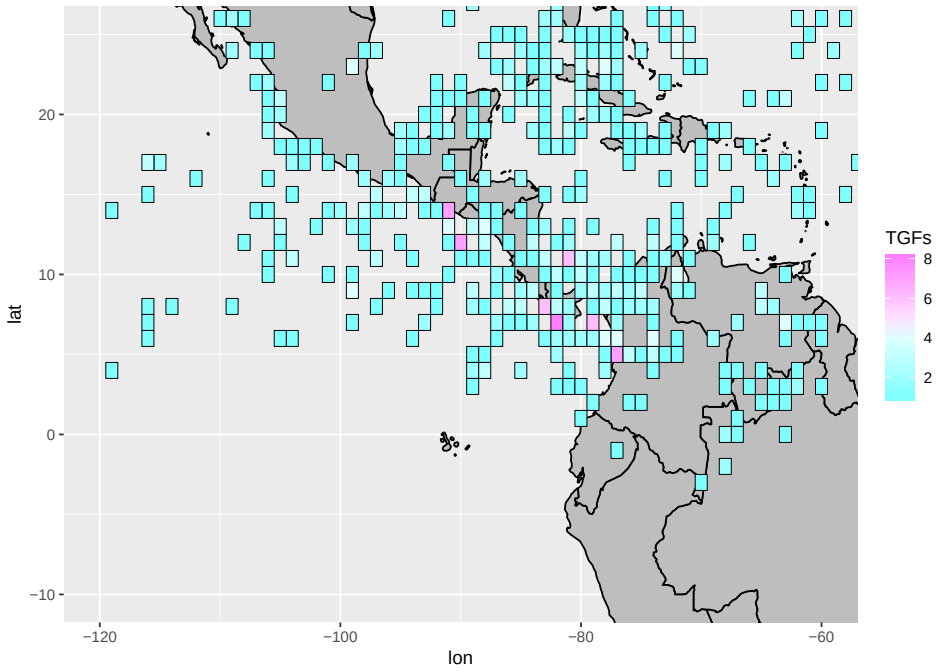

Figure 5. A tiled heat map showing TGFs detected by Fermi/WWLLN per square degree of latitude and longitude in Central America. Although the sample size is small, certain areas appear to be prone to higher TGF activity and could provide a starting point when searching for a candidate detector site.